JACS
JOURNAL OF THE AMERICAN CHEMICAL SOCIETY
Communication
pubs.acs.org/JACS

Efficient Photoelectrochemical Hydrogen Generation Using Heterostructures of Si and Chemically Exfoliated Metallic MoS_2

Qi Ding, Fei Meng, Caroline R. English, Miguel Cabán-Acevedo, Melinda J. Shearer, Dong Liang, Andrew S. Daniel, Robert J. Hamers, and Song Jin*

Department of Chemistry, University of Wisconsin − Madison, 1101 University Avenue, Madison, Wisconsin 53706, United States

Supporting Information

ABSTRACT: We report the preparation and characterization of highly efficient and robust photocathodes based on heterostructures of chemically exfoliated metallic 1T-MoS_2 and planar p-type Si for solar-driven hydrogen production. Photocurrents up to 17.6 mA/cm^2 at 0 V vs reversible hydrogen electrode were achieved under simulated 1 sun irradiation, and excellent stability was demonstrated over long-term operation. Electrochemical impedance spectroscopy revealed low charge-transfer resistances at the semiconductor/catalyst and catalyst/electrolyte interfaces, and surface photoresponse measurements also demonstrated slow carrier recombination dynamics and consequently efficient charge carrier separation, providing further evidence for the superior performance. Our results suggest that chemically exfoliated 1T-MoS_2/Si heterostructures are promising earth-abundant alternatives to photocathodes based on noble metal catalysts for solar-driven hydrogen production.

Hydrogen, a clean, storable, and high-energy density energy carrier, is a promising sustainable alternative for meeting the global energy demand and achieving an environmentally friendly fuel economy.[1] In the pursuit of utilizing renewable energy to produce hydrogen fuel, solar-driven water splitting is one of the most promising approaches.[2] This can be achieved by using either a photovoltaics-electrolyzer system or an integrated photoelectrochemical (PEC) system that couples the light harvesting and solar fuel production and enables direct solar-to-hydrogen production.[2] A PEC system has two essential components: a light absorber that generates electron−hole pairs upon illumination and an electrocatalyst that facilitates charge transfer and reduces the overpotential for fuel production. P-type silicon (p-Si) is an earth-abundant and inexpensive semiconductor with a suitable band gap (1.1 eV) and has been widely utilized as a light absorber in photocathodes.[3] Even though platinum and other noble metals remain the best electrocatalysts for hydrogen evolution reaction (HER),[4] the high cost and scarcity greatly limit their large scale deployment.[1a] The intensive search for earth-abundant, inexpensive, and nontoxic catalysts with comparable performance in HER has led to significant progress in the development of new catalysts recently, such as metal alloys,[5] chalcogenides,[6] nitrides,[7] phosphides,[8] borides,[9] and carbides.[10] Despite significant progress, most of these new materials have only been investigated as standalone electrocatalysts, and only a few have been integrated into photocathodes. The effective integration of electrocatalysts with light absorbers could potentially be quite challenging because of the semiconductor/catalyst chemical incompatibility and stability issues, induced interfacial defect states and recombination sites, or synthetic difficulties such as control over morphology, coverage, and thickness when growing the catalyst directly on the light absorber.[2b] One must also consider suitable band alignment and ensure efficient charge transfer across multiple interfaces. Several photocathodes based on non-noble metal catalysts for solar-driven HER have been recently reported;[5,11] however, their chemical stability and PEC performance still need to be improved. Developing low-cost photocathodes that could provide high efficiency as well as long-term stability for practical applications remains a significant challenge.

Among the earth-abundant HER catalysts, MoS_2 with a layered crystal structure has shown great promise.[6] A recent report showed that chemically exfoliated metallic 1T-MoS_2 nanosheets display dramatically enhanced catalytic activity compared to as-grown 2H-MoS_2.[6a] A simple *n*-butyl lithium (*n*-BuLi) treatment results in the phase conversion from semiconducting 2H-MoS_2 to metallic 1T-MoS_2, which has more facile electrode kinetics, proliferated active edge sites, and metallic transport.[6a] Built on these advantages, here we demonstrate integrated heterostructures of chemically exfoliated 1T-MoS_2 and planar p-Si as efficient and robust photocathodes for PEC hydrogen generation. A high current density of 17.6 mA/cm^2 at 0 V vs reversible hydrogen electrode (RHE) and an excellent onset of photocurrent are achieved together with good stability. Electrochemical impedance spectroscopy (EIS) and surface photoresponse (SPR) measurements further explain the superior performance of these 1T-MoS_2/Si photocathodes, making them promising earth-abundant alternatives to noble metal-based systems for solar-driven HER.

The simplest approach to assess the viability of 1T-MoS_2/Si heterostructures for PEC hydrogen generation is directly dropcasting 1T-MoS_2 nanosheet suspensions onto Si. We prepared 1T-MoS_2 suspensions by chemically exfoliating MoS_2 nanoflakes synthesized following the chemical vapor deposition (CVD) method we previously reported[6a] and harvesting the delaminated 1T-MoS_2 nanosheets, then dropcasting them onto preassembled planar p-Si photocathodes (resistivity 1−2.5 Ω cm) that were freshly etched in buffered HF (see Supporting Information for details and Figure S1 and S2 for SEM and Raman

Received: March 13, 2014
Published: May 24, 2014

dx.doi.org/10.1021/ja5025673 | J. Am. Chem. Soc. 2014, 136, 8504−8507

characterization). The photocurrent density−potential (J−E) data were collected using a three-electrode configuration in 0.5 M H_2SO_4 under simulated 1 sun irradiation (100 mW/cm^2) on Si photocathodes with increasing amount of 1T-MoS_2 suspension. Figure 1A shows that application of as little as 2

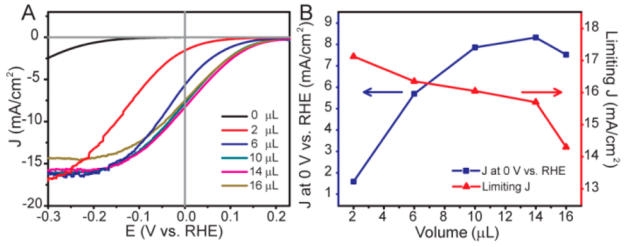

Figure 1. (A) J−E curve of p-Si photocathodes with different volume of dropcasted 1T-MoS_2 suspensions measured under simulated 1 sun irradiation. (B) Current density at 0 V vs RHE and limiting current density as a function of 1T-MoS_2 suspension volume.

μL of 1T-MoS_2 suspension could already significantly improve both the onset of photocurrent as well as the current density from those of bare p-Si. Gradually increasing the amount of the 1T-MoS_2 suspensions further shifted the onset of photocurrent to an even more positive value of +0.23 V vs RHE (compared to −0.14 V vs RHE for bare Si) and improved the current density at 0 V vs RHE to 8.5 mA/cm^2, before it reached a plateau and started to slightly decrease (Figure 1B, blue trace). While the catalytic activity improves with increasing catalyst loading, the overall performance can be reduced due to more light being blocked by MoS_2, as reflected in the decreasing limiting current density (red curve in Figure 1B). The optimal volume of MoS_2 suspension was shown to be 14 μL, corresponding to a loading density of ∼2.76 μg/cm^2 estimated by inductively coupled plasma atomic emission spectroscopy (ICP-AES) (Figure S3 and Table S1). As a comparison, the best current density at 0 V vs RHE obtained for Si photocathodes dropcasted with 2H-MoS_2 suspension was only 2.3 mA/cm^2, much lower than that of 1T-MoS_2 (the highest observed was 9.2 mA/cm^2). Nevertheless the same trend of peaking performance was observed as well (Figure S4).

With the promising result obtained from the simple dropcasting approach, we expect to further improve the PEC performance by directly growing MoS_2 onto Si to form a higher-quality interface between MoS_2 and Si. We developed a modified CVD synthesis, in which less precursors, lower temperature, and shorter reaction time (see SI for details) were employed than our previous protocol.[6a] This yielded a thin film of MoS_2 (40−80 nm thick) uniformly covering the Si substrate with sparse MoS_2 flakes standing out of the film (Figure 2A and inset). The amount of MoS_2 grown on Si was estimated to be ∼2.64 μg/cm^2 by ICP-AES (Table S1). The as-grown 2H-MoS_2 was then converted to metallic 1T-MoS_2 by n-BuLi treatment, and the phase change was confirmed by Raman and X-ray photoelectron spectroscopy (XPS). Characteristic Raman shifts at 387, 412, and 456 cm^{-1} were observed for as-grown 2H-MoS_2 samples, which correspond to in-plane E^1_{2g}, out-of plane A_{1g}, and longitudinal acoustic phonon modes, respectively.[12] After the n-BuLi treatment, three new shifts at 150, 219, and 327 cm^{-1} associated with the new vibration modes J_1, J_2, and J_3 of 1T-MoS_2 were observed.[6a,b,12] The significantly reduced intensity of 387 and 412 cm^{-1} shifts indicates that the content of 2H polymorph has been largely reduced (Figure 2C). We will simply use 1T-MoS_2 to refer to these chemically exfoliated samples thereafter. High-resolution

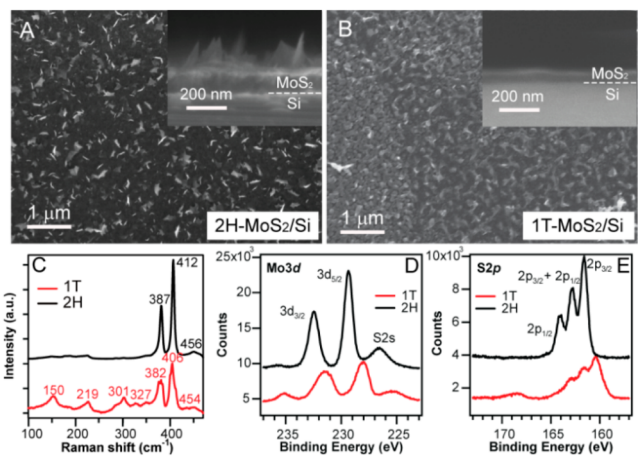

Figure 2. Comparison of top-down and cross-sectional (insets) SEM images of (A) 2H- and (B) 1T-MoS_2/Si, Raman spectra (C), high-resolution XPS of Mo3d (D) and S2p (E) regions for 2H- (black) and 1T- (red) MoS_2 on Si substrates.

XPS further revealed the lower binding energy of the Mo3d (Figure 2D) and S2p (Figure 2E) edges for the 1T-MoS_2. The $Mo3d_{5/2}$ and $Mo3d_{3/2}$ peaks shifted from ∼229.5 and ∼232.2 eV for the 2H-MoS_2 to ∼228.1 and ∼231.1 eV for the 1T-MoS_2, consistent with previous reports.[6b] Scanning electron microscopy (SEM) images of 1T-MoS_2/Si (Figure 2B) revealed that the MoS_2 thin film was maintained after the n-BuLi treatment, but became much more disordered and compressed compared to the as-grown 2H-MoS_2. The n-BuLi treatment was also performed on bare Si as a control experiment, and no noticeable change was detected either by SEM or in its PEC performance (Figure S5).

The PEC performance of as-grown 2H-MoS_2/Si and exfoliated 1T-MoS_2/Si heterostructures measured in 0.5 M H_2SO_4 under simulated 1 sun irradiation was compared in Figure 3A. Compared with bare Si photocathode which has an onset of photocurrent at −0.14 V vs RHE, the as-grown 2H-MoS_2/Si photocathode showed a shift in the onset of photocurrent to around +0.23 V vs RHE with a current density of 4.2 mA/cm^2 at 0 V vs RHE. The band bending of Si caused by 2H-MoS_2 is also shown by a solid-state diode measurement (Figure S6). A further substantial enhancement was observed for the 1T-MoS_2/Si. The onset of photocurrent shifted to +0.25 V vs RHE and the current density at 0 V vs RHE increased to 17.6 mA/cm^2, which is to our knowledge the highest reported photocurrent density for non-noble metal catalysts on planar p-Si photocathodes. Recently reported amorphous MoS_x on n^+p Si[11d] and Cu_2O[11e] photocathodes showed higher onset of photocurrent because of the buried junction and high built-in potential. However, the onset of photocurrent achieved here is already comparable to that of previously reported Pt on p-Si photocathode,[11f] and the current density achieved in the 1T-MoS_2 heterostructures is also higher than the amorphous MoS_x heterostructures.[11d,e] The observed fill factor is likely still hindered by nonoptimal MoS_2/Si interface but comparable to other reported p-Si photocathodes with non-noble metal catalysts.[5a,11a,b,f] Gas chromatography was used to measure generated H_2, and a Faradaic efficiency close to 100% was obtained, confirming that the generated photocurrent is indeed due to hydrogen evolution (Figure S7). Moreover, compared with dropcasted 1T-MoS_2/Si, the direct CVD grown 1T-MoS_2/Si photocathode had a more positive onset of photocurrent (0.25 V vs 0.23 V, both relative to RHE), a higher current density at 0 V vs RHE (17.6 mA/cm^2 vs 9.2 mA/cm^2),

dx.doi.org/10.1021/ja5025673 | J. Am. Chem. Soc. 2014, 136, 8504−8507

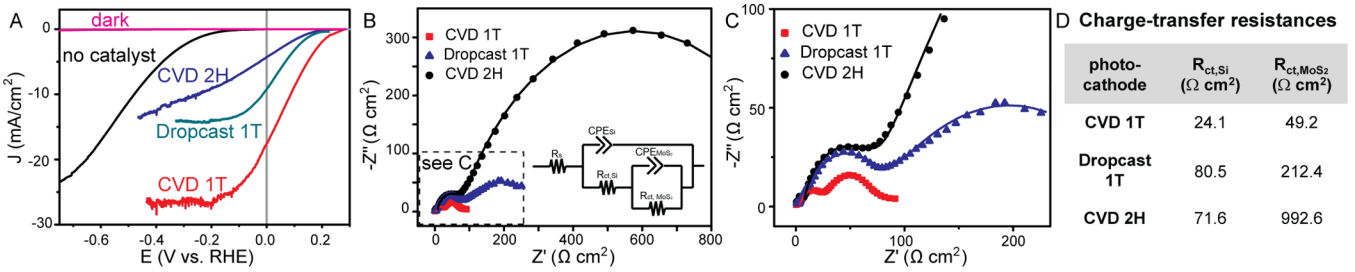

Figure 3. (A) *J*–*E* curves, (B, C) Nyquist impedance plots and (D) the fitted charge-transfer resistance values of a CVD grown 2H-MoS_2/Si photocathode (CVD 2H), a CVD grown 1T-MoS_2/Si photocathode (CVD 1T), and a dropcasted 1T-MoS_2/Si photocathode (dropcast 1T) measured in 0.5 M H_2SO_4 under simulated 1 sun irradiation. The *J*–*E* curve of a bare Si photocathode is also shown in A as a comparison. The dashed box in panel B is magnified in C. The solid line traces correspond to the fitting using the equivalent circuit in the inset of panel B.

and a higher limiting current density (26.7 mA/cm^2 vs 14.3 mA/cm^2).

To better understand the PEC performance, we performed EIS to elucidate the charge-transfer resistances in different photocathodes. Nyquist impedance plots for these photocathodes measured under illumination at 0.235 V vs RHE all display two distinguishable semicircles (Figure 3B,C). Following a reported example of catalyst-semiconductor system,[13] the data can be fitted to an equivalent circuit (Figure 3B inset) consisting of constant phase elements (CPE) associated with the semiconductor Si (CPE_{Si}) and the catalyst MoS_2 (CPE_{MoS2}) and charge-transfer resistances from Si to MoS_2 ($R_{ct,Si}$) and from MoS_2 to the redox couple in electrolyte ($R_{ct,\ MoS_2}$). The first semicircle on the left in the Nyquist plot yields $R_{ct,Si}$, which is a good indicator of the coupling between the light absorber (Si) and the catalyst (MoS_2); whereas the second semicircle on the right leads to $R_{ct,\ MoS_2}$, which usually reflects the catalytic activity of the material.

The charge-transfer resistances obtained from the fittings are summarized in Figure 3D with other parameters shown in Table S2. The charge-transfer resistance from MoS_2 to electrolyte ($R_{ct,\ MoS_2}$) of the CVD 1T-MoS_2/Si (49.2 Ω cm^2) is dramatically lower than that of the CVD 2H-MoS_2/Si (992.6 Ω cm^2), confirming the facile electrode kinetics of 1T-MoS_2/Si and further proving that the 1T phase is indeed much more catalytically active toward HER. The charge-transfer resistance from Si to MoS_2 ($R_{ct,Si}$) of the CVD 1T-MoS_2/Si (24.1 Ω cm^2) is also smaller than that of the CVD 2H-MoS_2/Si (71.6 Ω cm^2), likely due to more available electronic states in the metallic 1T phase relative to the semiconducting 2H phase.

Furthermore, the direct CVD grown 1T-MoS_2/Si heterostructure exhibits a much lower charge-transfer resistance from Si to MoS_2 (24.1 Ω cm^2) than the dropcasted 1T-MoS_2/Si (80.5 Ω cm^2), which confirms that the CVD grown MoS_2/Si heterostructure has a higher quality interface between the light absorber and catalyst. This is in good agreement with the observed superior performance of the CVD 1T-MoS_2/Si and highlights the benefits of direct CVD growth of catalysts on photocathodes for effective PEC system integration. Additionally, the impeded charge transfer from Si to MoS_2 as well as unoptimized MoS_2 morphology in the dropcasted 1T-MoS_2/Si result in larger $R_{ct,\ MoS_2}$ (212.4 Ω cm^2) than that of the CVD 1T-MoS_2/Si (49.2 Ω cm^2). Overall, the CVD 1T-MoS_2/Si has the smallest $R_{ct,\ MoS_2}$, followed by dropcasted 1T-MoS_2/Si and then CVD 2H-MoS_2/Si, which agrees with the trend of their *J*–*E* performance.

We further used time-resolved SPR spectroscopy to investigate the dynamics of the photogenerated charge carriers at the surface of the best performing CVD grown 1T-MoS_2/Si heterostructure. SPR can reveal information about the number of generated charges, charge separation at the interface as well as carrier lifetime.[14] Both bare p-Si and 1T-MoS_2/Si were measured in 0.5 M H_2SO_4 in a capacitor-like arrangement after illuminated with a brief laser pulse (details in SI). The recorded transient photocurrents (Figure S8) as well as integrated charges (Figure 4D) both show a rise of signal followed by a decay that can be fit

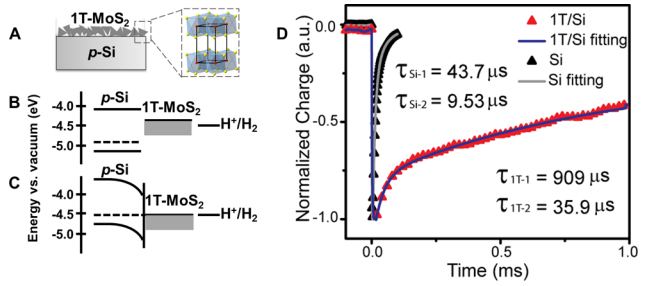

Figure 4. (A) Illustration of 1T-MoS_2 on p-Si. Schematic band energy diagram of p-Si, 1T-MoS_2, and H^+/H_2 redox couple at 0 V vs RHE in the dark before (B) and after (C) equilibrium. (D) Integrated TR-SPR spectra and corresponding biexponential fittings of 1T-MoS_2/Si (red and blue) and Si (black and gray).

to a multiple exponential function. For bare Si, negative signal was observed, indicating electrons accumulating at the surface, which is typical for a p-type material with downward band bending.[15] A biexponential fitting (details in SI) for the Si sample measured at 750 nm revealed time constants of τ_1 and τ_2 to be 9.53 and 43.7 μs, respectively, consistent with the reported value for p-Si at this doping level.[16] The 1T-MoS_2/Si heterostructure also exhibited negative signal implying similar downward band bending with p-Si, which is consistent with the band position[17] and band alignment between p-Si and 1T-MoS_2 (Figure 4B, 4C). A similar biexponential fitting yielded time constants of 35.9 and 909 μs, which shows that the 1T-MoS_2 layer dramatically increases the charge carrier lifetime of Si. This is likely due to the fast and irreversible electron transfer from Si to 1T-MoS_2, leaving holes behind in Si. This fast charge separation and slow charge recombination across the MoS_2/Si interface likely contribute to the efficient utilization of electrons for hydrogen evolution, and enable the superior PEC performance. Moreover, time-resolved microwave conductivity was also used to provide further insight into the carrier dynamics (SI and Figure S9).

Although 1T-MoS_2 is the thermodynamically metastable phase, these 1T-MoS_2/Si photocathodes remain stable and catalytically active over long-term operation. A chronoamper-

dx.doi.org/10.1021/ja5025673 | J. Am. Chem. Soc. 2014, 136, 8504–8507

ometry test of one CVD 1T-MoS_2/Si photocathode was performed at 0 V vs RHE over 3 h (Figure S10), and a 23% decrease in current density was observed, which is attributed to p-Si being oxidized during measurement as the current density could be readily recovered to its initial value after a buffered HF etch. Compared to a bare Si photocathode measured at the same condition,[11f] the degradation here has already been largely suppressed, suggesting that the MoS_2 coating might help to alleviate Si oxidation. Repeated scans of a CVD 1T-MoS_2/Si photocathode (Figure S11) and a dropcasted 1T-MoS_2/Si photocathode (Figure S12) also showed negligible decrease in performance. Furthermore, the current density at 0 V vs RHE of a CVD 1T-MoS_2/Si photocathode was monitored periodically over 70 days, and no noticeable decrease in performance was observed (Figure S13).

In summary, we have demonstrated that heterostructures of chemically exfoliated 1T-MoS_2 on planar p-Si behave as efficient and robust photocathodes for solar-driven HER, exhibiting an excellent onset of photocurrent and the highest current density at 0 V vs RHE for planar p-Si photocathodes with non-noble metal catalysts. EIS measurements demonstrated that the excellent performance of the CVD grown 1T-MoS_2/p-Si photocathodes can be attributed to small charge-transfer resistances across the semiconductor/catalyst and catalyst/electrolyte interfaces. SPR measurement also showed slow carrier recombination dynamics and efficient charge carrier separation. The excellent performance and stability make 1T-MoS_2/Si heterostructures promising alternatives to noble metal catalyst-based photocathodes for solar-driven hydrogen production and will stimulate further explorations of analogous metallic 1T polymorphs of layered metal chalcogenides for PEC solar energy conversion.

■ ASSOCIATED CONTENT

Supporting Information

Method details and supporting figures. This material is available free of charge via the Internet at http://pubs.acs.org.

■ AUTHOR INFORMATION

Corresponding Author

jin@chem.wisc.edu

Notes

The authors declare no competing financial interest.

■ ACKNOWLEDGMENTS

This research is supported by the U.S. Department of Energy, Office of Basic Energy Sciences, Division of Materials Sciences and Engineering, under Award DE-FG02-09ER46664. S.J. also thanks Research Corporation Scialog Award and the UW-Madison H. I. Romnes Faculty Fellowship for support. M.C. thanks the NSF Graduate Research Fellowship for support. We thank Donghyeon Kang and Prof. Kyoung-Shin Choi for assistance with GC.

■ REFERENCES

(1) (a) Lewis, N. S.; Nocera, D. G. *Proc. Natl. Acad. Sci. U.S.A.* **2006**, *103*, 15729. (b) Turner, J. A. *Science* **2004**, *305*, 972.

(2) (a) Walter, M. G.; Warren, E. L.; McKone, J. R.; Boettcher, S. W.; Mi, Q. X.; Santori, E. A.; Lewis, N. S. *Chem. Rev.* **2010**, *110*, 6446. (b) McKone, J. R.; Lewis, N. S.; Gray, H. B. *Chem. Mater.* **2014**, *26*, 407.

(3) (a) Reece, S. Y.; Hamel, J. A.; Sung, K.; Jarvi, T. D.; Esswein, A. J.; Pijpers, J. J. H.; Nocera, D. G. *Science* **2011**, *334*, 645. (b) Boettcher, S. W.; Spurgeon, J. M.; Putnam, M. C.; Warren, E. L.; Turner-Evans, D. B.; Kelzenberg, M. D.; Maiolo, J. R.; Atwater, H. A.; Lewis, N. S. *Science* **2010**, *327*, 185. (c) Boettcher, S. W.; Warren, E. L.; Putnam, M. C.; Santori, E. A.; Turner-Evans, D.; Kelzenberg, M. D.; Walter, M. G.; McKone, J. R.; Brunschwig, B. S.; Atwater, H. A.; Lewis, N. S. *J. Am. Chem. Soc.* **2011**, *133*, 1216.

(4) Khaselev, O.; Turner, J. A. *Science* **1998**, *280*, 425.

(5) (a) McKone, J. R.; Warren, E. L.; Bierman, M. J.; Boettcher, S. W.; Brunschwig, B. S.; Lewis, N. S.; Gray, H. B. *Energy Environ. Sci.* **2011**, *4*, 3573. (b) Warren, E. L.; McKone, J. R.; Atwater, H. A.; Gray, H. B.; Lewis, N. S. *Energy Environ. Sci.* **2012**, *5*, 9653.

(6) (a) Lukowski, M. A.; Daniel, A. S.; Meng, F.; Forticaux, A.; Li, L. S.; Jin, S. *J. Am. Chem. Soc.* **2013**, *135*, 10274. (b) Voiry, D.; Salehi, M.; Silva, R.; Fujita, T.; Chen, M. W.; Asefa, T.; Shenoy, V. B.; Eda, G.; Chhowalla, M. *Nano Lett.* **2013**, *13*, 6222−6227. (c) Wang, H.; Lu, Z.; Xu, S.; Kong, D. S.; Cha, J. J.; Zheng, G.; Hsu, P.; Yan, K.; Bradshaw, D.; Prinz, F. B.; Cui, Y. *Proc. Natl. Acad. Sci. U.S.A.* **2013**, *110*, 19701. (d) Li, Y. G.; Wang, H. L.; Xie, L. M.; Liang, Y. Y.; Hong, G. S.; Dai, H. J. *J. Am. Chem. Soc.* **2011**, *133*, 7296. (e) Kibsgaard, J.; Chen, Z. B.; Reinecke, B. N.; Jaramillo, T. F. *Nat. Mater.* **2012**, *11*, 963. (f) Laursen, A. B.; Kegnaes, S.; Dahl, S.; Chorkendorff, I. *Energy Environ. Sci.* **2012**, *5*, 5577. (g) Voiry, D.; Yamaguchi, H.; Li, J. W.; Silva, R.; Alves, D. C. B.; Fujita, T.; Chen, M. W.; Asefa, T.; Shenoy, V. B.; Eda, G.; Chhowalla, M. *Nat. Mater.* **2013**, *12*, 850. (h) Merki, D.; Fierro, S.; Vrubel, H.; Hu, X. L. *Chem. Sci.* **2011**, *2*, 1262. (i) Merki, D.; Hu, X. L. *Energy Environ. Sci.* **2011**, *4*, 3878. (j) Merki, D.; Vrubel, H.; Rovelli, L.; Fierro, S.; Hu, X. L. *Chem. Sci.* **2012**, *3*, 2515. (k) Lukowski, M. A.; Daniel, A. S.; English, C. R.; Meng, F.; Forticaux, A.; Hamers, R. J.; Jin, S. *Energy Environ. Sci.* **2014**, DOI: 10.1039/C4EE01329H.

(7) (a) Chen, W. F.; Sasaki, K.; Ma, C.; Frenkel, A. I.; Marinkovic, N.; Muckerman, J. T.; Zhu, Y. M.; Adzic, R. R. *Angew. Chem., Int. Ed.* **2012**, *51*, 6131. (b) Cao, B.; Veith, G. M.; Neuefeind, J. C.; Adzic, R. R.; Khalifah, P. G. *J. Am. Chem. Soc.* **2013**, *135*, 19186.

(8) Popczun, E. J.; McKone, J. R.; Read, C. G.; Biacchi, A. J.; Wiltrout, A. M.; Lewis, N. S.; Schaak, R. E. *J. Am. Chem. Soc.* **2013**, *135*, 9267.

(9) Vrubel, H.; Hu, X. L. *Angew. Chem., Int. Ed.* **2012**, *51*, 12703.

(10) Chen, W. F.; Wang, C. H.; Sasaki, K.; Marinkovic, N.; Xu, W.; Muckerman, J. T.; Zhu, Y.; Adzic, R. R. *Energy Environ. Sci.* **2013**, *6*, 943.

(11) (a) Hou, Y. D.; Abrams, B. L.; Vesborg, P. C. K.; Bjorketun, M. E.; Herbst, K.; Bech, L.; Setti, A. M.; Damsgaard, C. D.; Pedersen, T.; Hansen, O.; Rossmeisl, J.; Dahl, S.; Norskov, J. K.; Chorkendorff, I. *Nat. Mater.* **2011**, *10*, 434. (b) Berglund, S. P.; He, H.; Chemelewski, W. D.; Celio, H.; Dolocan, A.; Mullins, C. B. *J. Am. Chem. Soc.* **2014**, *136*, 1535. (c) Tran, P. D.; Pramana, S. S.; Kale, V. S.; Nguyen, M.; Chiam, S. Y.; Batabyal, S. K.; Wong, L. H.; Barber, J.; Loo, J. *Chem.—Eur. J.* **2012**, *18*, 13994. (d) Seger, B.; Laursen, A. B.; Vesborg, P. C. K.; Pedersen, T.; Hansen, O.; Dahl, S.; Chorkendorff, I. *Angew. Chem., Int. Ed.* **2012**, *51*, 9128. (e) Morales-Guio, C. G.; Tilley, S. D.; Vrubel, H.; Gratzel, M.; Hu, X. L. *Nat. Commun.* **2014**, DOI: 10.1038/ncomms4059. (f) Sim, U.; Yang, T. Y.; Moon, J.; An, J.; Hwang, J.; Seo, J. H.; Lee, J.; Kim, K. Y.; Lee, J.; Han, S.; Hong, B. H.; Nam, K. T. *Energy Environ. Sci.* **2013**, *6*, 3658. (g) Sun, Y.; Liu, C.; Grauer, D. C.; Yano, J.; Long, J. R.; Yang, P.; Chang, C. J. *J. Am. Chem. Soc.* **2013**, *135*, 17699.

(12) Sandoval, S. J.; Yang, D.; Frindt, R. F.; Irwin, J. C. *Phys. Rev. B* **1991**, *44*, 3955.

(13) Klahr, B.; Gimenez, S.; Fabregat-Santiago, F.; Bisquert, J.; Hamann, T. W. *J. Am. Chem. Soc.* **2012**, *134*, 16693.

(14) Kronik, L.; Shapira, Y. *Surf. Sci. Rep.* **1999**, *37*, 1.

(15) (a) Mahrov, B.; Boschloo, G.; Hagfeldt, A.; Dloczik, L.; Dittrich, T. *Appl. Phys. Lett.* **2004**, *84*, 5455. (b) Li, L. S.; Yu, Y. H.; Meng, F.; Tan, Y. Z.; Hamers, R. J.; Jin, S. *Nano Lett.* **2012**, *12*, 724. (c) Caban-Acevedo, M.; Faber, M. S.; Tan, Y. Z.; Hamers, R. J.; Jin, S. *Nano Lett.* **2012**, *12*, 1977.

(16) Tyagi, M. S.; Vanoverstraeten, R. *Solid-State Electron.* **1983**, *26*, 577.

(17) Yun, J. M.; Noh, Y. J.; Yeo, J. S.; Go, Y. J.; Na, S. I.; Jeong, H. G.; Kim, J.; Lee, S.; Kim, S. S.; Koo, H. Y.; Kim, T. W.; Kim, D. Y. *J. Mater. Chem. C* **2013**, *1*, 3777.